NANO LETTERS

2008
Vol. 8, No. 5
1451-1455

# Electrically Biased Nanolithography with KOH-Coated AFM Tips

**Jae-Won Jang, Raymond G. Sanedrin, Daniel Maspoch,† Seongpil Hwang, Tsuyohiko Fujigaya,‡ You-Moon Jeon, Rafael A. Vega, Xiaodong Chen, and Chad A. Mirkin***

*Department of Chemistry and International Institute for Nanotechnology, Northwestern University, 2145 Sheridan Road, Evanston, Illinois 60208-3113*

*Received February 12, 2008; Revised Manuscript Received February 27, 2008*

## ABSTRACT

**This letter provides the first study aimed at characterizing the desorption and nanolithographic processes for SAM-coated, gold-coated silicon substrates oxidatively patterned with an AFM with a tip under potential control. The process either results in recessed patterns where the monolayer has been removed or raised structures where the monolayer has been removed and silicon oxidation has taken place. Eleven different SAMs have been studied, and the type of pattern formed depends markedly upon SAM chain length, end functional group, and applied bias. We show how local pH and choice of monolayer can be used to very effectively control the type of pattern that is ultimately formed. Interestingly, we show that hydroxide anion accessibility to the substrate surface is one of the most significant factors in determining the pattern topography. Moreover, control over the pattern topography can be achieved by controlling the concentration of the KOH in the water meniscus formed at the point of contact between tip and surface in the context of a bias-controlled DPN experiment with a KOH-coated tip. The work provides important insight into the factors that control SAM desorption and also ways of controlling the topography of features made in a potential-controlled scanning probe nanolithographic process.**

A variety of scanning probe microscopy-based methods, such as dip-pen nanolithography (DPN),[1,2] nanografting,[3–5] and local oxidation or reduction nanolithography,[6–11] have been developed to nanopattern inorganic substrates. These methods often utilize self-assembled monolayers (SAMs) either as the pattern product[12–18] or resist material[19–21] to create the surface architectures of interest. When alkanethiol SAMs are used as a resist in local oxidation or reduction lithography on gold thin-film substrates, an interesting monolayer-dependent phenomenon has been observed.[22] When a negative bias is applied to the tip (and therefore positive to the substrate), a 16-mercaptohexadecanoic acid ($HS(CH_2)_{15}COOH$, MHA) monolayer can be oxidatively desorbed, leaving a recessed area on the substrate. In contrast, in the case of 1-octadecanethiol ($HS(CH_2)_{17}CH_3$, ODT), the monolayer is desorbed but there is also an oxidation of the underlying silicon, which results in the appearance of a raised structure, Scheme 1. Herein, we describe a study aimed at definitively characterizing the process, and we show how local pH and choice of monolayer can be used to effectively control the type of pattern that is ultimately formed. Interestingly, we show that hydroxide anion accessibility to the substrate surface is one of the most significant factors in determining the pattern topography (recessed or raised features). Moreover, control over the pattern topography can be achieved by controlling the concentration of the aqueous KOH ink in the context of the bias-controlled DPN experiment on MHA functionalized gold films.

**Scheme 1.** Schematic Diagram of (A) Recessed and (B) Protruded Pattern Formation

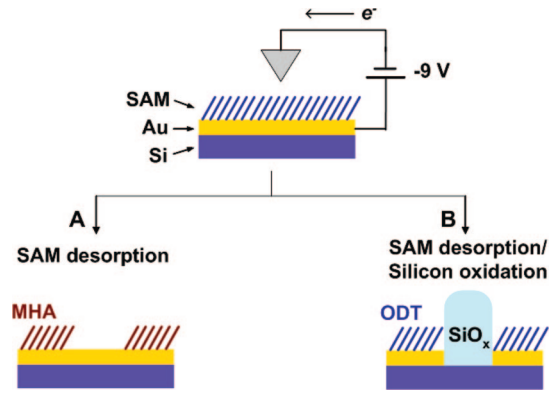


In a typical experiment, a series of alkanethiol SAMs on Au thin films were prepared by immersing a substrate in a 1 mM ethanolic solution of the corresponding alkanethiol for 1 h, followed by copious rinsing with ethanol and drying with $N_2$ (Table 1). The alkanethiol molecules used contained different terminal groups ($-CH_3$, $-COOH$, $-PO_3H_2$, $-OH$,

* Corresponding author. E-mail: chadnano@northwestern.edu. Fax: (+1)847-467-5123.
† Present address: Institut Català de Nanotecnologia, Campus Universitari de Bellaterra, 08193 Bellaterra, Spain.
‡ Present address: Department of Applied Chemistry, Kyushu University, Japan.

10.1021/nl080418b CCC: $40.75 
**Published on Web 04/01/2008**

**Table 1.** Number of Methylene Units, Patterning Onset Bias Voltage, Contact Angle by Water Droplet, and Pattern Geometry of All SAMs

| symbol in figure 1 | | number of methylene units | patterning onset bias voltage (V) | contact angle of water droplet (°) | pattern geometry (recess: −, raise: +) |
|---|---|---|---|---|---|
| A1 | $HS(CH_2)_{17}CH_3$ | 17 | −9 | 110.4 ± 0.9 | + |
| A2 | $HS(CH_2)_{15}CH_3$ | 15 | −7 | 107.0 ± 1.6 | + |
| A3 | $HS(CH_2)_{10}CH_3$ | 10 | −5 | 102.5 ± 1.0 | + |
| B1 | $HS(CH_2)_{15}COOH$ | 15 | −5 | 21.2 ± 1.3 | − |
| B2 | $HS(CH_2)_{10}COOH$ | 10 | −1 | 43.4 ± 1.3 | +[a] |
| C1 | $HS(CH_2)_{16}PO_3H_2$ | 16 | −9 | 57.0 ± 1.2 | − |
| C2 | $HS(CH_2)_{12}PO_3H_2$ | 12 | −7 | 45.0 ± 2.0 | + |
| D | $HS(CH_2)_{10}OH$ | 10 | −11 | 25.6 ± 0.5 | + |
| E | $HS(CH_2)_{11}NH_2$ | 11 | −5 | 40.5 ± 1.0 | + |
| F | $HS(CH_2)_{10}CF_3$ | 10 | −9 | 110.0 ± 2.0 | + |
| G | $HS(CH_2)_{11}EG_3OH$ | 20[b] | −7 | 27.8 ± 0.5 | + |

[a] Slightly recessed patterns are shown at −1, −3, and −5 V. [b] The EG ($OCH_2CH_2$) unit is counted as 3 methylene units.

$-NH_2$, $-CF_3$, and $-(OCH_2CH_2)_3OH$) and alkyl chain lengths (from 10 to 20 methylene units). Eight 2 $\mu$m long lines were written on each SAM with successively increasing applied bias voltages (−1 to −15 V with −2 V step) at a tip speed of 0.05 $\mu m \cdot s^{-1}$ under ambient conditions (~35% relative humidity, 23 °C), Figure 1. Alkanethiol SAMs with methyl end functional groups exhibit raised patterns, and these positive features appear at different bias voltages depending on the length of the alkanethiol used (Figure 1A1, A2, and A3). Indeed, patterns begin to form at −5, −7, and −9 V for 1-undecanethiol ($HS(CH_2)_{10}CH_3$, UDT, A3), 1-hexadecanethiol ($HS(CH_2)_{15}CH_3$, HDT, A2), and ODT (A1) SAMs, respectively. The recessed structures are never observed under these conditions. On the other hand, SAMs with carboxylic acid or phosphonic acid end functional groups exhibit a different behavior. For SAMs with these end groups, recessed patterns are formed at bias voltages between −5 and −20 V on SAMs with long alkyl chains (15 or 16 methylene units, Figure 1B1 and C1). Bias voltages greater than −20 V typically lead to raised patterns, diagnostic of $SiO_x$ formation (Figure S1 and S3, Supporting Information). However, if SAMs of molecules with the same end groups but shorter chain lengths are used, raised rather than recessed patterns are the product, even at low bias voltages (Figure 1B2 and C2). Moreover, the other alkanethiols SAMs show raised patterns at onset voltages that are dependent upon SAM end group (Figure 1D−G).

The recessed patterns are attributed to the desorption of alkanethiol SAMs, which is consistent with the work of Crooks et al.,[23,24] whereas raised patterns result from local oxidation of the silicon underneath the alkanethiol SAMs and gold film[25] (Supporting Information, Figure S1 and Scheme 1). This silicon oxidation formed via conductive atomic force microscopy (c-AFM) has been observed with monolayer-modified silicon substrates as well.[7,26–29] For ODT SAMs on Au-coated silicon substrates, both silicon oxidation and SAM desorption occur during the c-AFM experiment at a negative bias (see Supporting Information, Figure S2). The silicon oxidation is, in part, a product of the reaction of the substrate with hydroxide anion,[8–11,30] eq 1.

$$Si + 4OH^- \rightarrow SiO_2 + 2H_2O + 4e^- \quad (1)$$

Hydroxide anion can be generated at an AFM tip in the water meniscus through a reductive process,[10,30,31] eq 2.

$$4H_2O + 4e^- \rightarrow 2H_2 + 4OH^- \quad (2)$$

If hydroxide anions cannot access the silicon substrate, silicon oxidation is inhibited. Therefore, the accessibility of hydroxide anion to the silicon substrate is a significant factor for silicon oxidation by c-AFM scanning. Another factor to consider is the water layer between the AFM tip and SAMs,[32] especially because the water layer can affect electric field formation between the AFM tip and substrates during biasing.

To develop an understanding of the bias-controlled monolayer desorption and silicon oxidation processes, we investigated monolayers as a function of alkyl end functional group, chain length, and applied bias. Eleven different SAMs on Au thin films were prepared and characterized by contact angle measurements (Table 1). In addition, the topography of the patterns formed from a bias controlled tip was studied. All of the hydrophobic SAMs, regardless of chain length, after application of a negative bias to the tip showed raised structures, indicative of $SiO_x$ formation. Only the structures that can be deprotonated resulted in recessed patterns, and whether or not a raised or recessed structure was observed was highly dependent upon alkyl chain length. For example, MHA and 16-mercaptohexadecylphosphonic acid ($HS(CH_2)_{16}PO_3H_2$, MHPA) show recessed patterns, which begin to form at −5 and −9 V, respectively, Figure 1B1,C1. 11-Mercaptoundecanoic acid ($HS(CH_2)_{10}COOH$, MUA) and 12-mercaptododecylphosphonic acid ($HS(CH_2)_{12}PO_3H_2$, MDPA) also show protruded patterns but at onset voltages −7 V, parts B2 and C2 of Figure 1, respectively.

As stated above, for alkanethiol SAMs with methyl end functional groups, protruded patterns form at higher biases. Indeed, an increase in chain length corresponds with a more negative bias required to effect silicon oxidation and formation of the raised patterns, Figure 2. Also, as the number of methylene groups increases, an increase in both measured contact angle and patterning onset bias voltage is observed. For SAMs comprised of linear alkanes, it is known that longer alkyl chains typically lead to higher monolayer packing densities[33,34] and the formation of more hydrophobic surfaces. Therefore, the accessibility of hydroxide anions to the underlying Si substrate is expected to be more limited for longer SAMs for both steric and hydrophobic reasons. In addition, this is also consistent with the observation that SAMs with longer alkyl chains have higher junction resistances.[35] Therefore, longer chain lengths lead to less injected

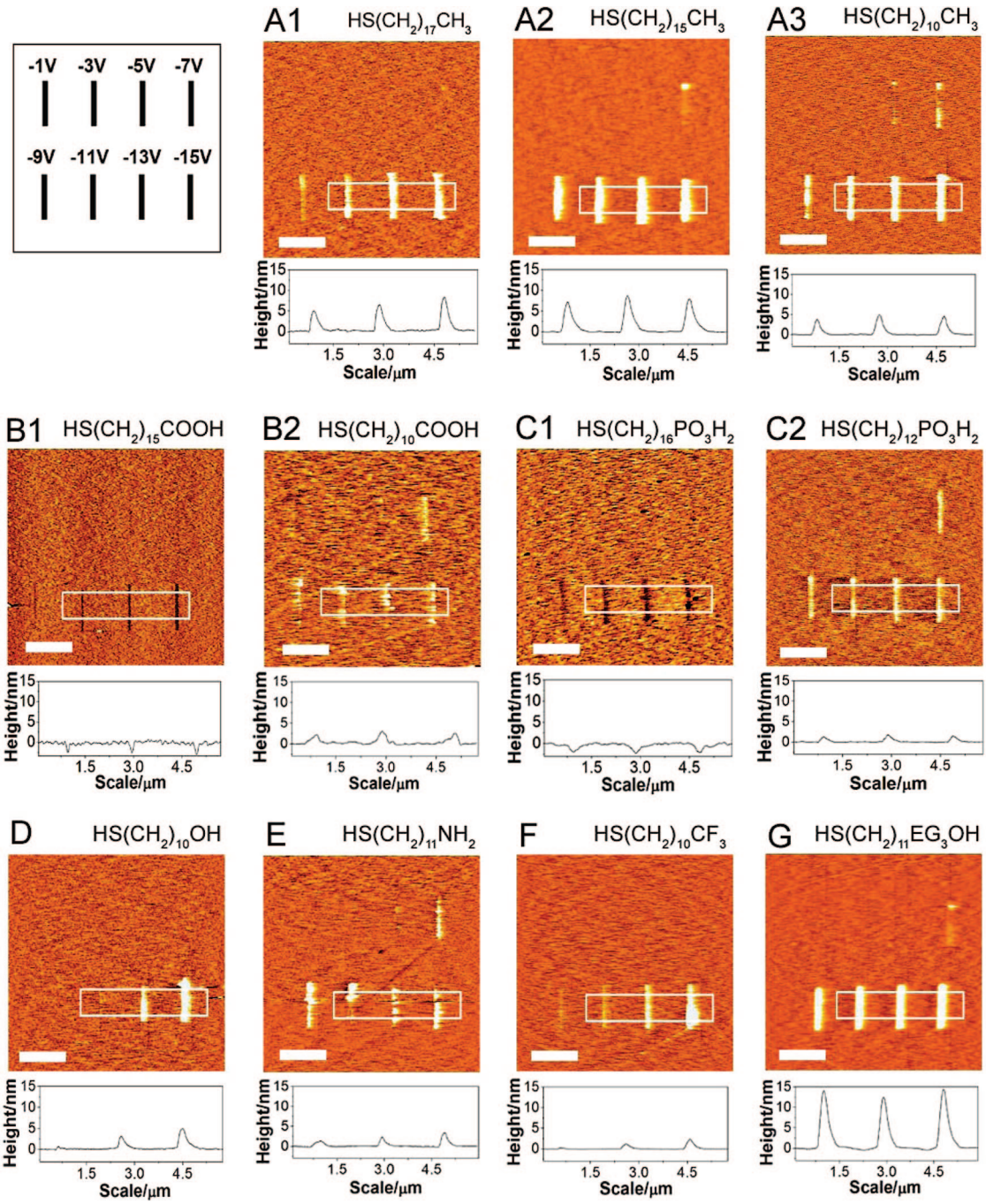


**Figure 1.** Contact-mode AFM (CM-AFM) topographic images of 2 $\mu$m long lines at bias voltages in the range of −1 to −15 V on several alkanethiol SAMs written by c-AFM. (A) Images of $CH_3$-terminated SAMs: (A1) 1-octadecanethiol ($HS(CH_2)_{17}CH_3$, ODT), (A2) 1-hexadecanethiol ($HS(CH_2)_{15}CH_3$, HDT), (A3) 1-undecanethiol ($HS(CH_2)_{10}CH_3$, UDT). (B) Images of COOH-terminated SAMs: (B1) 16-mercaptohexadecanoic acid ($HS(CH_2)_{15}COOH$, MHA), (B2) 11-mercaptoundecanoic acid ($HS(CH_2)_{10}COOH$, MUA). (C) Images of $PO_3H_2$-terminated SAMs: (C1) 16-mercaptohexadecylphosphonic acid ($HS(CH_2)_{16}PO_3H_2$, MHPA), (C2) 12-mercaptododecylphosphonic acid ($HS(CH_2)_{12}PO_3H_2$, MDPA). Images of (D) 11-mecapto-1-undecanol ($HS(CH_2)_{10}OH$, MDO), (E) 11-aminoundecanethiol ($HS(CH_2)_{11}NH_2$, AUT), (F) 11-perfluoroundecanethiol ($HS(CH_2)_{10}CF_3$, PFUT), and (G) 11-mercaptoundecyltri(ethylene glycol) ($HS(CH_2)_{11}EG_3OH$, PEG-SH) SAMs, respectively. Schematic diagram (top and left corner) illustrates the overall experimental process. Height profiles are obtained from analysis of highlighted regions in each image. They represent average heights across the regions scanned. Scale bars are 2 $\mu$m. The height scales for all images are 5 nm.

current and lower amounts of hydroxide anion formation (eq 2). Similar trends are observed for SAMs with carboxylic acid and phosphonic acid end functional groups. For such SAMs, the patterning onset bias voltage also increases with increasing alkyl chain length (Table 1, compare Figure 1 B1 with B2 and C1 with C2). Interestingly, with long alkyl chain lengths, recessed rather than raised patterns are observed for this class of molecules. For the carboxylic acid and phosphonic acid terminated structures, we hypothesize that hydroxide anion accessibility to the substrates is more limited than their shorter chain analogues because of the electrostatic repulsion between the negatively charged end

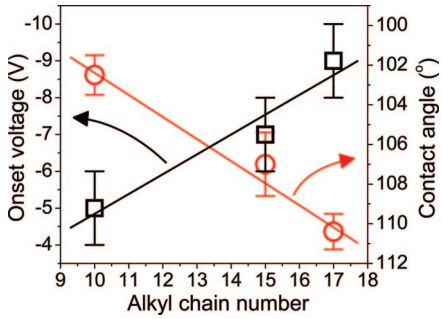


**Figure 2.** Alkyl chain length dependent patterning onset bias voltage (□) and contact angle value (○) of $CH_3$-terminated SAMs.

**Scheme 2.** Schematic Diagrams Describing the Interactions between the $OH^-$ and the (A) MHA SAM-Coated and (B) ODT SAM-Coated Surfaces [a]

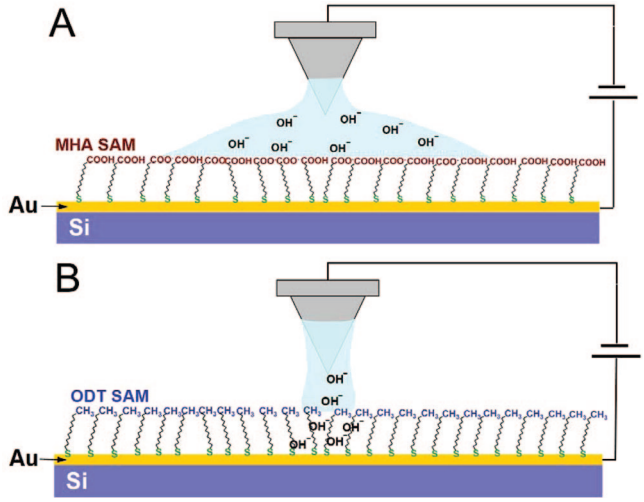


[a] The deprotonated acids create an electrostatic barrier for the $OH^-$ in the case of the MHA-SAM.

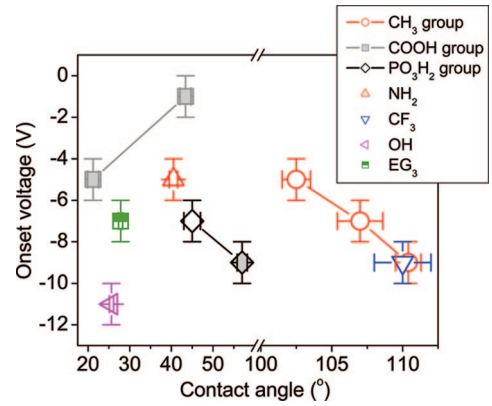


**Figure 3.** Contact angle-dependent patterning onset bias voltages for all SAMs in Table 1. Solid markers represent recessed patterns. Open markers represent raised patterns. There is no apparent correlation between the water contact angles of the SAMs and the patterning onset voltages.

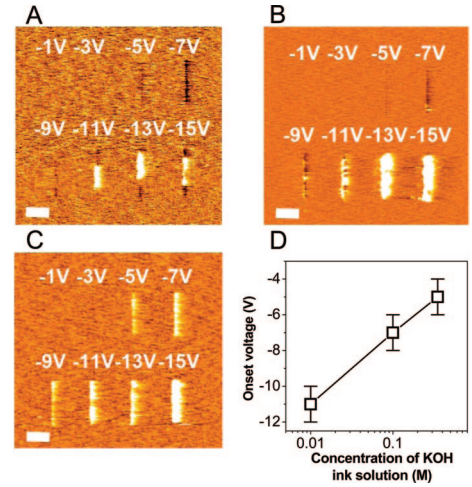


**Figure 4.** CM-AFM topography images of MHA SAMs patterned with a tip coated with solutions of different KOH concentrations: (A) 0.01 M, (B) 0.1 M, and (C) 0.35 M. The patterning process was the same one used in Figure 1. Scale bars are 1 $\mu$m. The height scales of all images are 5 nm. (D) A graph of positive feature patterning onset voltage as a function of the concentration of KOH in the solution used to coat the tip.

functional groups and the hydroxide anion, which inhibits silicon oxidation, Scheme 2. In other words, the more loosely packed monolayers allow hydroxide ions to reach the surface and effect the silicon oxide formation, while the more densely packed monolayers made of the longer chain alkanethiols limit the amount of hydroxide formed and the accessibility to the underlying surface. Of course, this is a kinetically controlled process. If one rewrites over the recessed pattern, silicon oxidation takes place because there is no longer a monolayer protecting the surface (see Supporting Information, Figure S3B).

Importantly, there seems to be no relationship between the onset voltage and the contact angle of the monolayer prior to applied bias, Figure 3. This suggests that the water meniscus that forms at the point of contact between tip and sample[32,36] is not the major factor in SAM patterning by c-AFM scanning. All likely have water at the point of contact,[32,36] but the amount does not significantly affect the ability of hydroxide ions to penetrate the SAM and form silicon oxide.

To test the importance of hydroxide ions on this monolayer desorption and subsequent silicon oxidation process, we studied the patterning process with a KOH-coated tip, Figure 4. Specifically, contact-mode AFM (CM-AFM) was used to pattern a surface coated with a MHA SAM using tips coated with aliquots of aqueous 0.01, 0.1, and 0.35 M KOH, respectively. Without KOH-coated tips, recessed patterns are observed, consistent with monolayer desorption but little or no silicon oxidation, regardless of bias voltage studied, Figure 1B1. With KOH-coated tips, raised patterns consistent with silicon oxidation are observed at higher bias voltages; the bias voltage transition from recessed to raised patterns depends upon KOH concentration. With higher concentrations, lower bias voltages are required, Figure 4D. Indeed, the voltage required to effect silicon oxidation is exponentially and inversely proportional to the concentration of the KOH inking solution.

In conclusion, we have investigated the factors controlling the oxidative removal and subsequent oxidation of SAM-coated, gold-coated silicon substrates. Hydroxide anion accessibility to the substrate surface and bias voltage seem to be the critical factors affecting the type of pattern that is

formed. High hydroxide ion concentrations and shorter chain lengths favor silicon oxidation, and negatively charged SAM end groups can be used to further inhibit the silicon oxidation process. These data help explain this unusual process and moreover point toward a way of controlling it in a lithographic manner.

**Acknowledgment.** C.A.M. acknowledges the AFOSR, DARPA, and NSF for financial support of this research. J.-W.J. acknowledges support from the Korea Research Foundation Grant (KRF-M01-2005-000-10321-0). S.H. acknowledges support from the Korea Research Foundation Grant funded by the Korean Government (MOEHRD) (KRF-2006-214-C00060). D.M. thanks to the Ministerio de Ciencia y Tecnologia for a Ramón y Cajal contract.

**Supporting Information Available:** Experimental section. Characterization details for raised and recessed patterns. This material is available free of charge via the Internet at http://pubs.acs.org.

## References

(1) Piner, R. D.; Zhu, J.; Xu, F.; Hong, S. H.; Mirkin, C. A. *Science* **1999**, *283*, 661–663.
(2) Ginger, D. S.; Zhang, H.; Mirkin, C. A. *Angew. Chem., Int. Ed.* **2004**, *43*, 30–45.
(3) Xu, S.; Miller, S.; Laibinis, P. E.; Liu, G.-Y. *Langmuir* **1999**, *15*, 7244–7251.
(4) Amro, N. A.; Xu, S.; Liu, G.-Y. *Langmuir* **2000**, *16*, 3006–3009.
(5) Liu, M.; Liu, G.-Y. *Langmuir* **2005**, *21*, 1972–1978.
(6) Kim, Y. T.; Bard, A. J. *Langmuir* **1992**, *8*, 1096–1102.
(7) Sugimura, H.; Hanji, T.; Hayashi, K.; Takai, O. *Adv. Mater.* **2002**, *14*, 524–526.
(8) Ma, Y.-R.; Yu, C.; Yao, Y.-D.; Liou, Y.; Lee, S.-F. *Phys. Rev. B* **2001**, *64*, 195324.
(9) Avouris, P.; Hertel, T.; Martel, R. *Appl. Phys. Lett.* **1997**, *71*, 285–287.
(10) Dagata, J.; Schneir, J.; Harary, H. H.; Evans, C. J.; Postek, M. T.; Bennett, J. *Appl. Phys. Lett.* **1990**, *56*, 2001–2003.
(11) Garcia, R.; Martinez, R. V.; Martinez, J. *Chem. Soc. Rev.* **2006**, *35*, 29–38.
(12) Hoeppener, S.; Schubert, U. S. *Small* **2005**, *1*, 628–632.
(13) Liu, X.; Fu, L.; Hong, S. H.; Dravid, V. P.; Mirkin, C. A. *Adv. Mater.* **2002**, *14*, 231–234.
(14) Fresco, Z. M.; Frechet, J. M. J. *J. Am. Chem. Soc.* **2005**, *127*, 8302–8303.
(15) Liu, S.; Maoz, R.; Sagiv, J. *Nano Lett.* **2004**, *4*, 845–851.
(16) Vega, R. A.; Maspoch, D.; Salaita, K.; Mirkin, C. A. *Angew. Chem., Int. Ed.* **2005**, *44*, 6013–6015.
(17) Rozhok, S.; Shen, C. K.-F.; Littler, P.-L. H.; Fan, Z.; Liu, C.; Mirkin, C. A.; Holz, R. C. *Small* **2005**, *1*, 445–451.
(18) Lee, K.-B.; Park, S.-J.; Mirkin, C. A.; Smith, J. C.; Mrksich, M. *Science* **2002**, *295*, 1702–1705.
(19) Zhang, H.; Mirkin, C. A. *Chem. Mater.* **2004**, *16*, 1480–1484.
(20) Zhang, H.; Chung, S.-W.; Mirkin, C. A. *Nano Lett.* **2003**, *3*, 43–45.
(21) Weinberger, D. A.; Hong, S.; Mirkin, C. A.; Wessels, B. W.; Higgins, T. B. *Adv. Mater.* **2000**, *12*, 1600–1603.
(22) Jang, J.-W.; Maspoch, D.; Fujigaya, T.; Mirkin, C. A. *Small* **2007**, *3*, 600–605.
(23) Schoer, J. K.; Crooks, R. M. *Langmuir* **1997**, *13*, 2323–2332.
(24) Schoer, J. K.; Zamborini, F. P.; Crooks, R. M. *J. Phys. Chem.* **1996**, *100*, 11086–11091.
(25) Hwang, J. S.; You, Z. Y.; Lin, S. Y.; Hu, Z. S.; Wu, C. T.; Chen, C. W.; Chen, K. H. *Appl. Phys. Lett.* **2005**, *86*, 161901.
(26) Hoeppener, S.; van Schaik, J. H. K.; Schubert, U. S. *Adv. Funct. Mater.* **2006**, *16*, 76–82.
(27) Wouters, D.; Willems, R.; Hoeppener, S.; Flipse, C. F. J.; Schubert, U. S. *Adv. Funct. Mater.* **2005**, *15*, 938–944.
(28) Ara, M.; Graaf, H.; Tada, H. *Appl. Phys. Lett.* **2002**, *80*, 2565–2567.
(29) Li, Q.; Zheng, J.; Liu, Z. *Langmuir* **2003**, *19*, 166–171.
(30) Bloeb, H.; Staikov, G.; Schultze, J. W. *Electrochim. Acta* **2001**, *47*, 335–344.
(31) Sugimura, H.; Uchida, T.; Kitamura, N.; Masuhara, H. *J. Phys. Chem.* **1994**, *98*, 4352–4357.
(32) Piner, R. D.; Mirkin, C. A. *Langmuir* **1997**, *13*, 6864–6868.
(33) Nagarajan, R. *Langmuir* **2002**, *18*, 31–38.
(34) Fenter, P.; Eberhardt, A.; Liang, K. S.; Eisenberger, P. *J. Chem. Phys.* **1997**, *106*, 1600–1608.
(35) Engelkes, V. B.; Beebe, J. M.; Frisbie, C. D. *J. Am. Chem. Soc.* **2004**, *126*, 14287–14296.
(36) Rozhok, S.; Piner, R.; Mirkin, C. A. *J. Phys. Chem. B* **2003**, *107*, 751–757.

NL080418B